Solid State Communications 162 (2013) 23–27

Contents lists available at SciVerse ScienceDirect

Solid State Communications

journal homepage: www.elsevier.com/locate/ssc

Pseudo-gap opening and Dirac point confined states in doped graphene

J.E. Barrios-Vargas, Gerardo G. Naumis *

Depto. de Física-Química, Instituto de Física, Universidad Nacional Autónoma de México (UNAM), Apdo. Postal 20-364, 01000 México D.F., México

ARTICLE INFO

Article history:
Received 27 November 2012
Received in revised form
26 February 2013
Accepted 5 March 2013
by V. Pellegrini
Available online 13 March 2013

Keywords:
A. Graphene
A. Disordered graphene
D. Electronic properties
D. Magnetic properties

ABSTRACT

The appearance of a pseudo-gap and the build up of states around the Dirac point for doped graphene can be elucidated by an analysis of the density of states spectral moments. Such moments are calculated by using the Cyrot-Lackmann theorem, which highlights the importance of the network local topology. Using this approach, we sum over all disorder realizations up to a certain radius to show how the spectral moments change. As a result, the spectrum becomes unimodal, however, strictly localized states appears at the Dirac point. Such states are important for the magnetic properties of graphene, and are calculated as a function of the doping concentration. By removing these states in the count of the spectral moments, it is finally seen that the density of states increases its bimodal character and the tendency for a pseudo-gap opening. This result is important to understand the trends in the magnetic and electronic properties of doped graphene. In graphene with vacancies, the same ideas can also be useful to isolate in a rough way which effects are due solely to topology.

Graphene is currently a 'rising star' in condensed-matter physics [1]. Mainly, because it is the first truly two-dimensional crystal [2], and has a high electrical [3] and thermal conductivity [4]. These properties place graphene as an ideal candidate for a new electronic, based in carbon, to replace silicon. The problem is that graphene is not a semiconductor. However, it has been shown that graphene can present a change from metal to insulator when it is doped by adsorbed H [5], as was also predicted by using arguments on frustration due to the graphene's underlying triangular symmetry [6,7]. It is important to remark that such theoretical results, were performed under the supposition that hydrogen is bonded to graphene covalently with the $2p_z$ orbital, and very roughly, it confines the wave function spatially like a vacancy [8,9]. Although this approach may seems too simplistic, it has been useful to predict localization tendencies and the size of a pseudo-gap [6], in good agreement with experimental data [5]. More recent detailed calculations show that in fact, vacancies and impurities are different, both requiring a fine tuning of the tight-binding Hamiltonian [10,11], instead of using an infinite self-energy at impurity sites. For example, nitrogen and boron have a scattering potential with a extension larger than 10 shells of neighbors [10]. However, the exercise of considering impurity sites with infinite self-energy is interesting because it allows to understand which effects are due solely to the honeycomb lattice topology. For low concentration of impurities, this procedure leads to resonant states near the Dirac energy [12], E_D, which coincides with the Fermi energy for a zero bias potential. For higher concentrations, a region of localized and critical states appears [6,13]. Such critical states are believed to be multifractal [13]. Numerical simulations suggest that a pseudo-gap is open at the Dirac point [6]. On the other hand, in the middle of the pseudo-gap, states appears as the impurity concentration raises. Such states are important to understand the diamagnetic properties of graphene [14]. Some of these features are robust against the specific parameters of disorder since they only depend on general symmetry arguments [15]. So for example, more detailed calculations will shift the pseudo-gap or its size, but the basic mechanism is provided by topology [6,7]. More refined results can be obtained by performing a systematic series expansion for finite impurity self-energy. Here we present only the first and dominant term of such serie, others are corrections to it. Also, renormalization techniques can be used to treat local disorder in non-diagonal elements [6,13].

In the same spirit, here we show that the appearance of the pseudo-gap and the build up of states around E_D can be elucidated by an analysis of the spectral moments [16] which highlights the importance of the network local topology. Furthermore, this method allows to count the number of states at E_D as a function of the concentration, and explain them, above the percolation threshold, as strictly confined states in local clusters.

As a model, consider the graphene's honeycomb lattice with substitutional impurities placed at random with a uniform distribution. The corresponding tight-binding Hamiltonian for the electron in the π orbital is given by [17],

$$\mathcal{H} = -t\sum_{\langle \boldsymbol{i}\boldsymbol{j}\rangle} |\boldsymbol{i}\rangle\langle\boldsymbol{j}| + \varepsilon\sum_{\ell} |\ell\rangle\langle\ell|, \tag{1}$$

* Corresponding author. Tel.: +52 56 22 51 74; fax: +52 56 22 50 08.
E-mail address: naumis@fisica.unam.mx (G.G. Naumis).

0038-1098/$ - see front matter © 2013 Elsevier Ltd. All rights reserved.
http://dx.doi.org/10.1016/j.ssc.2013.03.006

where the first sum is over nearest neighbors, $t=2.79$ eV is the hopping energy [18], and the second is over every impurity sites with self-energy ε. The number of impurities sites, N_{imp}, is determined by the concentration $C=N_{\text{imp}}/N$, where N is the total sites on the honeycomb lattice. It is well known that for pure graphene ($\varepsilon=0$), the density of states (DOS) is bimodal, i.e., the two Van Hove singularities dominate in the DOS. We will show that the bimodal behavior tends to increase when the concentration is increased, although one must be careful since states at the middle of the spectrum (at E_{D}) have a weight that needs to be removed first.

To prove this, we will consider here the moments of the DOS function $\rho(E)$. The spectral moments are defined as

$$\mu_{\boldsymbol{i}}^{(n)}=\int_{-\infty}^{\infty}(E-\mathcal{H}_{\boldsymbol{ii}})^{n}\rho_{\boldsymbol{i}}(E)\,dE. \tag{2}$$

These moments can be calculated by counting closed paths that start and return at the same lattice site $\boldsymbol{i}$, as was shown by Cyrot-Lackman [19],

$$\mu_{\boldsymbol{i}}^{(n)}=\langle \boldsymbol{i}|(\mathcal{H}-\mathcal{H}_{\boldsymbol{ii}})^{n}|\boldsymbol{i}\rangle, \tag{3}$$

since the right hand term of the equation corresponds to the number of paths with n steps that return to the original site $\boldsymbol{i}$.

There is a dimensionless parameter to measure the tendency of the local DOS (LDOS) to open a pseudo-gap at its center [19],

$$s_{\boldsymbol{i}}=\frac{\mu_{\boldsymbol{i}}^{(4)}\mu_{\boldsymbol{i}}^{(2)}-(\mu_{\boldsymbol{i}}^{(2)})^{3}-(\mu_{\boldsymbol{i}}^{(3)})^{2}}{(\mu_{\boldsymbol{i}}^{(2)})^{3}} \tag{4}$$

If $s_{\boldsymbol{i}}\geq 1$ the LDOS is unimodal; meanwhile, if $s_{\boldsymbol{i}}<1$ the LDOS is bimodal, and has a tendency for a pseudo-gap opening at the center [19].

Also, it is important to remark that here, no self-energy $\mathcal{H}_{\boldsymbol{ii}}$ was considered for carbon atoms in the unperturbed Hamiltonian. Thus, the zero energy has been chosen to coincide with the vertices of the Dirac cone at E_{D}. As a result, the spectrum is symmetric around $E=0$. The real spectrum can be readily obtained by an energy shifting, as usually done in all works concerning graphene.

Let us now consider first the case of pure graphene. The sites are undistinguished, i.e. DOS=LDOS, and therefore we can toggle off the site index $\boldsymbol{i}$ and calculate the moments. It is easy to see that

- $\mu^{(0)}=1$ due to the normalization condition.
- $\mu^{(1)}=0$.
- $\mu^{(2)}=3t^{2}$ and is proportional to the coordination of each site, Z=3 (Fig. 1).
- $\mu^{(3)}=0$, because the electron can not return to the original site with 3 steps. The same holds for any odd spectral moment. Thus, any bipartite lattice always has a symmetric spectrum, as for example, in the Penrose lattice (vertex model) [20].

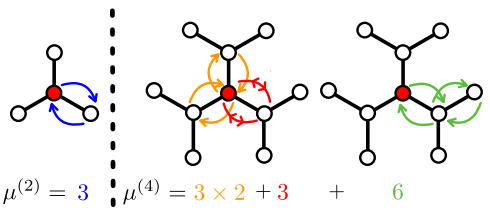

Fig. 1. (Color online) Sketch of the path counting for the honeycomb lattice. Left panel, a two step path that returns to the original site. Right panel, four step paths are divided in revisiting (red and orange), and no revisiting (green) to the original site. The red paths go from the origin to a neighboring site and come back and visit the same site neighbor. The orange paths go from the origin to a neighboring site, come back and visit another neighbor.

- $\mu^{(4)}=15t^{4}$ after counting the four steps paths (Fig. 1), that revisit and not revisit the original site.

From the previous considerations, $s=2/3$ for pure graphene, and this value corresponds to a bimodal DOS.

If there is a concentration of impurities, C, the problem is much more difficult. However, here we are interested in impurities which take one electron from the π orbital leaving almost a hole. We will model this case assuming $t/\varepsilon\ll 1$. It is important to remark that more detailed calculations show that impurities or vacancies present a more complex behavior. For example, nitrogen and boron involve a significant modification of the diagonal elements of the matrix only, while a vacancy can be modeled [10] using $\varepsilon=10$ eV and $t_{1\text{J}}=1.9$ eV (compared with $t=2.7$ eV for pristine graphene). Here we will consider the case $t/\varepsilon\ll 1$. In spite of this, one can include in a natural way a smaller ε by performing a series expansion in powers of t/ε using the same techniques [21]. Thus, here we are computing the lowest order term of the serie. This case corresponds to the split band limit, and bands are suitable to be studied in a separate way [21]. The reason is that the wavefunctions of the graphene band do not have amplitude on impurities, while for the impurity band the opposite is true. This can be proved in general, and corrections are easy to find using a t/ε expansion of the wavefunction [21]. Here, we will restrict our calculations to the graphene band, using a restricted Hamitonian,

$$\mathcal{H}_{\mathbf{cc}}=-t\sum_{\langle \boldsymbol{i},\boldsymbol{j}\rangle\in\mathbf{cc}}|\boldsymbol{i}\rangle\langle\boldsymbol{j}|, \tag{5}$$

where the sum over $\boldsymbol{i}$ and $\boldsymbol{j}$ is carried only over carbon sites (indicated by the subindex **cc**), with DOS $\rho_{\mathbf{cc}}(E)$. A similar Hamiltonian can be written for the impurity band, $\mathcal{H}_{\mathbf{ib}}$ with DOS given by $\rho_{\mathbf{ib}}(E)$. The total DOS is $\rho(E)=\rho_{\mathbf{cc}}(E)+\rho_{\mathbf{ib}}(E)$. In what follows, we will consider only the DOS and spectral moments of $\mathcal{H}_{\mathbf{cc}}$, so for simplicity, we drop any subindex **cc**. The impurity band can be easily obtained from $\mathcal{H}_{\mathbf{cc}}$ by considering the behavior for concentrations $1-C$ and a shift of the spectrum by ε.

Now we define the moments averages over all disorder realizations, i.e., for all the possible combinations of impurities sites (ℓ) and carbon sites as

$$\langle\mu^{(n)}\rangle=\sum_{\boldsymbol{j}_1,\ldots\boldsymbol{j}_{n-1}\neq\ell}P(\boldsymbol{i}\boldsymbol{j}_1,\ldots\boldsymbol{j}_{n-1})\times\mathcal{H}_{\boldsymbol{i}\boldsymbol{j}_1}\mathcal{H}_{\boldsymbol{j}_1\boldsymbol{j}_2}\ldots\mathcal{H}_{\boldsymbol{j}_{n-1},\boldsymbol{i}} \tag{6}$$

where $P(\boldsymbol{i}\boldsymbol{j}_1,\ldots\boldsymbol{j}_{n-1})$ is the probability of each path made only from carbon atoms.

In order to obtain $\langle s\rangle$, we need to calculate $\langle\mu^{(2)}\rangle$ and $\langle\mu^{(4)}\rangle$. Again $\langle\mu^{(3)}\rangle=0$ since the lattice defined on pure carbon sites is bipartite. Notice that this property only holds for $t/\varepsilon\ll 1$. Now we perform the calculation of the first moments by summing over all statistical realizations of disorder.

The second moment, $\langle\mu^{(2)}\rangle$, can be counted by noting that there are four possible configurations with impurities and non-impurities for nearest neighbors (Fig. 2). Following the diagram in the figure, it is easy to see that the statistical distribution of configurations is a binomial. It follows that the second moment is just the average coordination of the network ($\langle Z\rangle$), obtained from the binomial distribution:

$$\langle\mu^{(2)}\rangle=t^{2}\sum_{Z=0}^{3}\binom{3}{Z}C^{3-Z}(1-C)^{Z}Z=3t^{2}(1-C). \tag{7}$$

where Z denote the coordination of a site. This value gives an excellent approximation to the graphene band width.

For the fourth moment, we chose a Carbon site and again we divide our count on paths which revisit the original site and those which do not revisit. Fig. 3 shows schematically the possible

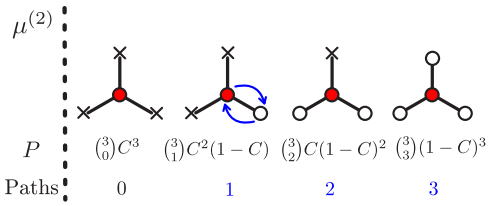

Fig. 2. (Color online) Outline of the count of two step paths. P is the probability of the configuration and Paths denotes the number of paths for each configuration with the same statistical weight. The open circles denote carbon sites, and the crosses, impurity sites which have zero amplitude for energies in the Carbon band. The starting site is the filled circle.

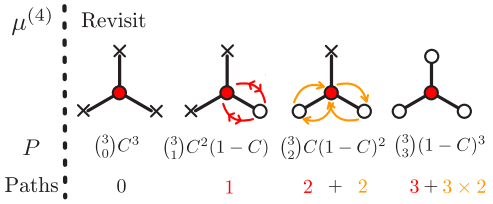

Fig. 3. (Color online) Outline of the path counting that revisit the original site using four steps. P is the probability of the configuration and Paths denotes the number of paths for each configuration. The red paths go from the origin to a neighboring site and come back and visit the same site neighbor. The orange paths go from the origin to a neighboring site and come back and visit another neighbor site. The open circles correspond to carbon sites while impurity sites are denoted by crosses.

configurations and paths that revisit the original site, hence,

$$\text{Revisit} = t^4 \sum_{Z=0}^{3} \binom{3}{Z} C^{3-Z}(1-C)^Z Z^2 = 3t^4(1-C)(3-2C). \tag{8}$$

The paths which do not revisit the original site can be calculated noting that those are classified into two basic configurations, one with a maximum possible coordination $Z=3$ and a second with $Z=2$. Therefore,

$$\text{No revisit} = 3t^2(1-C) \times 2t^2(1-C) = 6t^4(1-C)^2. \tag{9}$$

Thus, $\langle \mu^{(4)} \rangle$ is given by

$$\langle \mu^{(4)} \rangle = \text{Revisit} + \text{No revisit} = 3t^4(1-C)(5-4C). \tag{10}$$

Finally, the averaged dimensionless parameter is

$$\langle s \rangle = \frac{1}{3}\left(\frac{2-C}{1-C}\right). \tag{11}$$

which is plotted in Fig. 4 as a function of the impurity concentration. Also, in the same figure we show the dimensionless parameter $\langle s \rangle_{\text{num}}$, calculated numerically from a direct diagonalization of the Hamiltonian. Such diagonalization was performed using periodic boundary conditions in all directions. The results were done in an ensemble of 100 disorder realizations, for lattices of 20,000 sites using $\varepsilon = 10^4$. To perform the diagonalization, the Intel Math Kernel Library was used. Finally, the moments were calculated using that

$$\langle \mu^{(n)} \rangle = \frac{1}{N}\sum_{m}^{N} E_m^n, \tag{12}$$

where the index m is such that E_m belongs to the **cc** band, i.e. $E_m \in (-3t, 3t)$. As can be seen, the match between the numerical results and our local topology analytical computation is excellent.

Paradoxically, we have found that the DOS becomes unimodal when the impurity concentration is greater than 0.5, a fact which seems to suggest that the DOS around the center of the spectrum is rising. To solve this conflict, we observe that impurities lead to a peak at zero energy, i.e., at the Dirac energy. Notice that only when the impurity self-energy is infinite, one gets strictly a peak at zero, since the solution of the Lifshitz equation for resonant states [7]

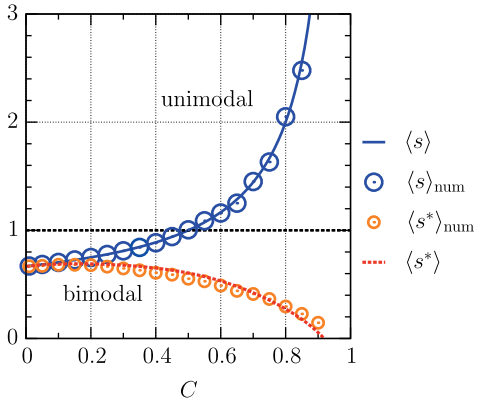

Fig. 4. (Color online) The dimensionless parameter $\langle s \rangle$ and $\langle s^* \rangle$ as a function of C. The lines correspond to the analytical calculation using Eqs. (11) and (15). The symbols are obtained from the numerical calculation, showing an excellent agreement with the analytical results. If $\langle s \rangle \geq 1$ the DOS is unimodal, meanwhile if $\langle s \rangle < 1$ the DOS is bimodal. Once the zero energy states are removed, $\langle s^* \rangle$ shows a decreasing bimodality indicating a pseudo-gap opening.

goes to zero as $1/\varepsilon$. Thus, in the case of big but finite ε, the solution can be slightly shifted from zero. We have verified this point by using different values of ε, and the shifting of the DOS to higher frequencies is reduced systematically. It is known that states at zero frequency are due to an imbalance between impurity sites on each of the sublattices [22]. In general, their number is just given by $N_A - N_B$ where N_A and N_B is the number of impurities on each of the graphene's bipartite sublattices, usually denoted by A and B. For these states, the amplitude is zero on each sublattice, as required from a simple renormalization of the Hamiltonian [6,7]. Such states are known to occur in other bipartite lattices, like in random binary alloys [21,23] or in the Penrose lattices [20]. Here we calculate the number of such states, and at the same time, we will consider a modified density of states, DOS*, which does not take into account these states. In such a way, we can separate the behavior of the DOS depending whether one includes or not the weight of confined states. The moments of the DOS* can be calculated by excluding zero energy states

$$\langle \mu^{(n)^*} \rangle = \frac{1}{N^*}\sum_{m}^{N^*} E_m^n. \tag{13}$$

where N^* is the total number of sites with energy different from zero. This moment can be related to the previous

$$\langle \mu^{(n)^*} \rangle = \frac{N}{N^*}\langle \mu^{(n)} \rangle = \frac{1}{1-f_0}\langle \mu^{(n)} \rangle, \tag{14}$$

where $f_0 \equiv (N-N^*)/N$ is the density of states for energy zero. f_0 is function of the concentration, C. Hence, we can evaluate the parameter $\langle s^* \rangle$ as

$$\langle s^* \rangle = (1-f_0)\langle s \rangle - f_0. \tag{15}$$

$\langle s^* \rangle$ also is plotted in Fig. 4 as a function of the impurity concentration using two ways of computing f_0, one using a direct count form diagonalization and the other using an approximation detailed below. Note that $\langle s^* \rangle \to 0$ when $C \to 1$. This indicates that the DOS* tends to increase its bimodality, and results in a pseudo-gap in the DOS. Numerically, the evolution of the DOS can be shown in Fig. 5, where it is clear how the central peak of confined states grows with the number of impurities, while a pseudo-gap appears. From a physical point of view, the pseudo-gap, the Van Hove singularity and the central peak are due to the underlying triangular symmetry of the lattice, which leads to frustration, and as usual, there is a pushing of states while degeneration increases [7].

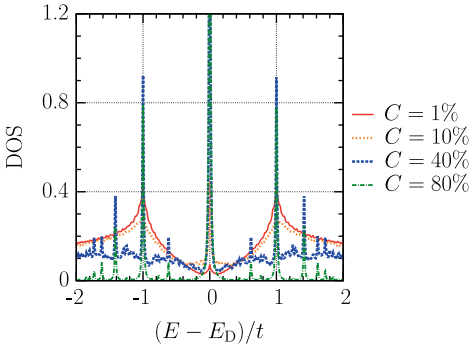

Fig. 5. (Color online) DOS of the carbon band for different concentration of impurities, as obtained from diagonalization averaging over 100 realizations of disorder for a network of N=20,000 sites, using $\varepsilon=10^4$.

Finally, in order to estimate the number of states at energy zero, we observe that their number depends on N_A–N_B as has been previously explained. However, the problem is how to compute N_A–N_B as a function of the concentration. For the very low concentration range, Pereira et al. [22] gave the following expression:

$$P(C)=\frac{C^2}{(1-C)} \tag{16}$$

Notice that we modified the original expression found by Pereira et al. [22] by a C, since our results are normalized only to one of the subbands. In Fig. 7 we compare Eq. (16) with our numerical results, showing a good agreement only for $C<0.2$. For higher values, the formula does not fit at all the numerical results. The disagreement is due to the fact that near the percolation threshold, zero states are dominated by clusters delimited by impurities, as shown in Fig. 6. These states are confined and occur in pure carbon atom clusters with the property that the wave function is zero in the boundary of the cluster. Thus, it is natural to start looking for these clusters in the limit $C\to1$. Zero energy states in clusters have three properties: (1) the amplitude in one of the bipartite sublattices is zero, (2) the sum of the amplitude of all neighbors for any site is always zero, and (3) impurities act as zeros. We can calculate the contribution of the smallest atoms clusters, which are the most probable as $C\to1$, and compare with the numerical result. Schematically, the few atoms clusters are shown in Fig. 6, together with its contribution as a function of the impurity concentration.

The fraction of states at zero energy taking into account the smallest clusters are specifically:

- for one atom $f_0^{(1)}=C^3$,
- up to three atoms $f_0^{(3)}=C^3+3C^5(1-C)^2$,
- up to six atoms $f_0^{(6)}=C^3+3C^5(1-C)^2+C^6(1-C)^3+6C^7(1-C)^4+15C^8(1-C)^5$.

These contributions of few atoms clusters are compared in Fig. 7 with the fraction obtained from diagonalization. As expected, for C close to one, the one atom cluster ($f_0^{(1)}$) gives an excellent approximation, while the inclusion of three atoms clusters ($f_0^{(3)}$) and six atoms clusters ($f_0^{(6)}$) allows to obtain a better approximation as C goes to zero. It is clear that this analysis requires bigger and bigger clusters, making the calculation much more difficult as $C\to0$. However, since we have the solution found by Pereira et al., it is better to perform an interpolation in between both limits. By using the Levenberg-Marquardt algorithm [24], we obtain

$$F(C)=C^2(1-C)^{\alpha-1}+f_0^{(6)}C^{\alpha} \tag{17}$$

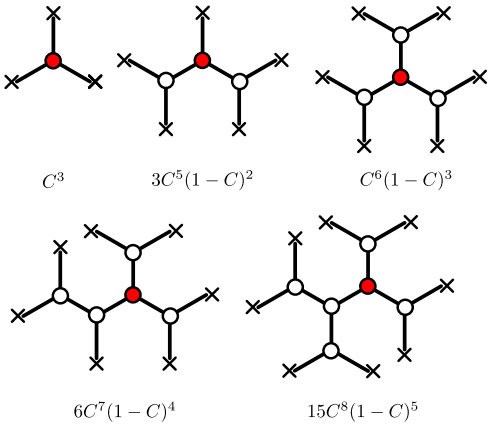

Fig. 6. (Color online) Sketch of the clusters with confined states and its contribution to the fraction of states at energy zero as a function of C. Carbon sites are denoted by circles, and impurities by crosses. Around any carbon site, the sum of the neighbors amplitudes is zero.

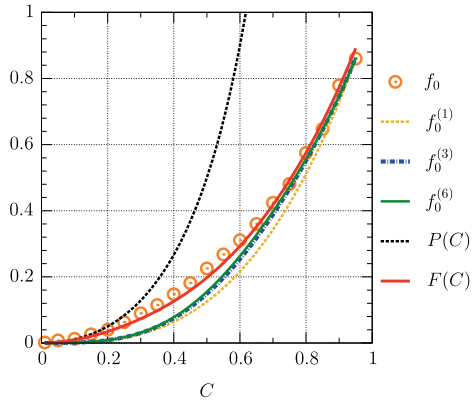

Fig. 7. (Color online) Fraction of states at zero energy, f_0 as a function of the impurity concentration obtained from numerical diagonalization of the Hamiltonian, compared with the one atom cluster ($f_0^{(1)}$) approximation, and the inclusion of three atoms clusters ($f_0^{(3)}$) and six atoms clusters ($f_0^{(6)}$). The Pereira et al. formula [22] given by Eq. (16) and the interpolation given by Eq. (17) are also shown for comparison.

with $\alpha=1.73$. The comparison between Eq. (17) and the numerical results appears in Fig. 7, showing a very good agreement in the whole concentration range.

In conclusion, we have obtained analytically the first spectral moments of doped graphene, and the approximate number of states at the Dirac energy. By removing these states, it is possible to see a tendency to open a pseudo-gap as a function of an increased concentration of impurities. The states at the Dirac point and the pseudo-gap are important to determine the magnetic and electronic properties of doped graphene.

Acknowledgments

We thank the DGAPA-UNAM project IN-102513. J.E. Barrios-Vargas acknowledges the scholarship from CONACyT (Mexico).

References

[1] A.K. Geim, K.S. Novoselov, Nat. Mater. 6 (3) (2007) 183–191, http://dx.doi.org/10.1038/nmat1849.
[2] K.S. Novoselov, D. Jiang, F. Schedin, T.J. Booth, V.V. Khotkevich, S.V. Morozov, A.K. Geim, Proc. Natl. Acad. Sci. USA 102 (30) (2005) 10451–10453, http://dx.doi.org/10.1073/pnas.0502848102.

[3] K.S. Novoselov, A.K. Geim, S.V. Morozov, D. Jiang, Y. Zhang, S.V. Dubonos, I.V. Grigorieva, A.A. Firsov, Science 306 (5696) (2004) 666–669, http://dx.doi.org/10.1126/science.1102896.
[4] A.A. Balandin, S. Ghosh, W. Bao, I. Calizo, D. Teweldebrhan, F. Miao, C.N. Lau, Nano Lett. 8 (3) (2008) 902–907, http://dx.doi.org/10.1021/nl0731872.
[5] A. Bostwick, J.L. McChesney, K.V. Emtsev, T. Seyller, K. Horn, S.D. Kevan, E. Rotenberg, Phys. Rev. Lett. 103 (2009) 056404, http://dx.doi.org/10.1103/PhysRevLett.103.056404.
[6] G.G. Naumis, Phys. Rev. B 76 (2007) 153403, http://dx.doi.org/10.1103/PhysRevB.76.153403.
[7] J.E. Barrios-Vargas, G.G. Naumis, J. Phys.: Condens. Matter 23 (37) (2011) 375501, http://dx.doi.org/10.1088/0953-8984/23/37/375501.
[8] J. Katoch, J.-H. Chen, R. Tsuchikawa, C.W. Smith, E.R. Mucciolo, M. Ishigami, Phys. Rev. B 82 (2010) 081417, http://dx.doi.org/10.1103/PhysRevB.82.081417.
[9] N.M.R. Peres, Rev. Mod. Phys. 82 (2010) 2673–2700, http://dx.doi.org/10.1103/RevModPhys.82.2673.
[10] A. La Magna, I. Deretzis, G. Forte, R. Pucci, Phys. Rev. B 80 (2009) 195413, http://dx.doi.org/10.1103/PhysRevB.80.195413.
[11] I. Deretzis, G. Fiori, G. Iannaccone, A. La Magna, Phys. Rev. B 81 (2010) 085427, http://dx.doi.org/10.1103/PhysRevB.81.085427.
[12] J.E. Barrios-Vargas, G.G. Naumis, Philos. Mag. 91 (29) (2011) 3844–3857, http://dx.doi.org/10.1080/14786435.2011.594457.
[13] J.E. Barrios-Vargas, G.G. Naumis, J. Phys.: Condens. Matter 24 (25) (2012) 255305, http://dx.doi.org/10.1088/0953-8984/24/25/255305.
[14] T. Espinosa-Ortega, I.A. Luk'yanchuk, Y.G. Rubo, Superlattice Microstruct. 49 (3) (2011) 283–287, http://dx.doi.org/10.1016/j.spmi.2010.06.018.
[15] F. Evers, A.D. Mirlin, Rev. Mod. Phys. 80 (2008) 1355–1417, http://dx.doi.org/10.1103/RevModPhys.80.1355.
[16] F. Cyrot-Lackmann, J. Phys. Chem. Solids 29 (7) (1968) 1235–1243, http://dx.doi.org/10.1016/0022-3697(68)90216-3.
[17] P.R. Wallace, Phys. Rev. 71 (1947) 622–634, http://dx.doi.org/10.1103/PhysRev.71.622.
[18] S. Reich, J. Maultzsch, C. Thomsen, P. Ordejón, Phys. Rev. B 66 (2002) 035412, http://dx.doi.org/10.1103/PhysRevB.66.035412.
[19] A. Sutton, Electronic Structure of Materials, Oxford Science Publications, Oxford University Press, USA, 1993.
[20] G.G. Naumis, R.A. Barrio, C. Wang, Phys. Rev. B 50 (1994) 9834–9842, http://dx.doi.org/10.1103/PhysRevB.50.9834.
[21] S. Kirkpatrick, T.P. Eggarter, Phys. Rev. B 6 (1972) 3598–3609, http://dx.doi.org/10.1103/PhysRevB.6.3598.
[22] V.M. Pereira, J.M.B. Lopes dos Santos, A.H. Castro Neto, Phys. Rev. B 77 (2008) 115109, http://dx.doi.org/10.1103/PhysRevB.77.115109.
[23] G.G. Naumis, C. Wang, R.A. Barrio, Phys. Rev. B 65 (2002) 134203, http://dx.doi.org/10.1103/PhysRevB.65.134203.
[24] J. Nocedal, S. Wright, Numerical Optimization, Springer Series in Operations Research Series, Springer-Verlag GmbH, 1999.